University of North Carolina Asheville
Journal of Undergraduate Research
Asheville, North Carolina
February 2018

Characterizing *Kepler* Objects of Interest with Multicolor Photometry and Change-Point Analysis

Nathan Kirse
Department of Physics
University of North Carolina Asheville
One University Heights
Asheville, North Carolina 28804 USA

Faculty Advisors: Dr. Brian Dennison & Dr. Britt Lundgren

Abstract

We report follow-up observations of seven *Kepler* Objects of Interest (KOIs) from the remote controlled 0.61-m telescope at the Sierra Stars Observatory in California. We alternated between broadband photometric filters (NI-R-V-B) to measure transit events of KOIs in two distinct colors. We could then compare light curves (LCs) between filters in order to test for astrophysical false positive scenarios. Due to limitations directly resulting from the small aperture of the Sierra Stars Observatory telescope (SSOT) and magnitude of *Kepler* stars (between V∼15 and V∼18), LCs had a large root-mean-square (rms) scatter. In consequence, claims about the disposition of all seven KOIs lack statistical certainty in this study. However, change-point analysis (CPA) has proven to be an effective tool when parameterizing LCs. This technique has not been used before in exoplanetary transit LCs, and is worth comparing to other methods.

1 Introduction and Concept Theory

NASA's *Kepler* mission, which began in 2009, has produced more exoplanet discoveries than any other mission/survey to date. Paradoxically, the great success of *Kepler* in producing thousands of exoplanet candidates (4496 as of January 2018 according to the NASA Exoplanet Archive) has presented a new kind of challenge to astronomers. Before the *Kepler* telescope, discovering exoplanets was a slow and arduous process which usually required sufficient transit measurements as well as radial velocity (RV) measurements before a candidate could be considered a bonafide exoplanet.[5] However, this is not feasible given the large quantity of *Kepler* candidates and low intensity of the stars, and as a result, many *Kepler* candidates remain unconfirmed. Present spectrographic technology lacks the precision needed to detect the minuscule RV shifts of host stars from low mass *Kepler* candidates. Since trusted detection methods such as the RV method are often unattainable, this has forced astronomers to instead rule out possible false-positive scenarios to as a way of vetting. This is described in Morton et al. 2016 as probabilistic validation.[5] Many of these false-positive scenarios, such as a blended system (a background eclipsing binary is one example), are a direct result of the poor spatial resolution of the *Kepler* telescope (nearly 4 arc-seconds per pixel), which is a consequence of its large field of view. Larger telescopes (both ground-based and space-based) with exceptional spatial resolution can help rule out the possibility of blended systems.[3]

Tingley 2004 proposes a method that probes for blended systems not by taking high-resolution images, but by analyzing the color of transits.[1] In the scenario that a true planet-star transit is observed, we should expect no difference in the transit depth between optical bands since planets practically emit no light of their own. However, if a transit is the product of a hidden eclipsing binary, and the two stars differ in color, we should expect the transit depth to depend on the optical band in which it is observed. Unlike the high-resolution imaging technique, this method does not require state-of-the-art observatories since it is simply looking for a color dependence in the transit depth. A couple studies have implemented this technique, such as Colòn et al. 2010, except with narrow-band photometric measurements as opposed to broadband.[2,4] This study will attempt to demonstrate a possible transit color dependence by alternating broadband photometric filters.

2 Observations

The 0.61-m (24 inch) telescope at the Sierra Stars Observatory (SSO) is located near Markleeville, CA, which is approximately 30 miles south of Carson City, NV. Carson City causes a small amount of light pollution in the northern hemisphere. SSO's 0.61m telescope was remotely controlled at an offsite location. The imaging instrument of SSO is a Finger Lakes Instrumentation ProLine camera (FLIP). It contains a Kodak KAF-09000 3056 x 3056 pixel CCD chip. The 12-micron pixels give an image scale of 0.4 arcseconds/pixel unbinned, and a 21 x 21 arc minutes field of view. FLIP offers four Astrodon SCHÜLER Johnsons-Cousins 50mm square filters (Infrared, Red, Visible (green), Blue) for photometry.

We observed a total of 12 transits from seven *Kepler* Objects of Interest (KOI) during the summer months of 2016. Parameters such as the transit midpoint and transit duration were found by using the Transit and Ephemeris Service on the NASA Exoplanet Archive in order to schedule observations. Observation runs ranged from 4 to 5 hours, and exposures lasted 60 to 300 seconds depending on the transit duration and stellar magnitude of the KOI, respectively. Dead time between exposures was thirty seconds across all observations. The FLIP CFW-4-5 filter wheel allowed us to efficiently alternate between two filters during every observation (this is indicated by the $\rightleftharpoons$ symbol in the Filters column of Table 1). Initially, the red and blue filters were chosen for a high-contrast effect, but the intrinsic redness of most KOI stars made longer wavelength filters more practical. Thus, infrared (near infrared), red, and visible (green) were used most often. Poor stellar tracking was a major issue for SSO since target centroid shifts of over 100 pixels were common.

3 Data Reduction

AstroImageJ64 (AIJ) was the primary tool used for multi-aperture photometry. A range of aperture sizes for target and reference stars were tested. For most KOIs, an aperture radius of 5 pixels was settled on to minimize the out-of-transit (OOT) root-mean-square (rms) scatter in LCs. This radius was consistent for both reference and target stars. What's more, the same reference stars and aperture radii were used per KOI. For the annulus, an inner radius of 20 pixels and an outer radius of 40 pixels was used for all KOI observations. However, the annulus size proved to have insignificant changes on the rms scatter of the OOT LC. Reference stars were chosen pseudo-randomly based off their proximity to the target star (the poor tracking of SSO made it so that any star not near the image center was likely to exit the FOV), and reference stars must have a similar flux to the target star (to ensure that no single reference star would dominate relative flux measurements). Outliers within LCs were always the result of hot or cold pixels in the CCD. Due to the poor tracking of SSO, these defective pixels would often pass in and out of photometric apertures. This was always correlated with an outlier, so other causes were not pursued.

4 Light Curve Analysis

Flux measurement errors provided by AIJ were not used in the statistical analysis of LCs. The magnitude of these errors implied a much larger rms scatter than what was actually observed in the LCs (standard

All Observations						
Date (2016)	Target	Filters	Exposure (sec)	Observation (hours)	RA (degrees)	Dec (degrees)
June 21st	KOI-3749.01	R ⇌ B	90	5	285.007720	49.503979
June 22nd	KOI-0883.01	R ⇌ B	90	4	296.683070	42.967869
June 23rd	KOI-1654.01	R ⇌ B	90	5	283.796540	49.503990
June 30th	KOI-1326.01	R ⇌ B	30	5	286.834870	39.760849
July 15th	KOI-1654.01	R ⇌ V	90	5	283.796540	49.503990
July 16th	KOI-1654.01	R ⇌ V	90	5	283.796540	49.503990
July 28th	KOI-3119.01	NI ⇌ V	300	4	296.587190	40.722988
August 3rd	KOI-3749.01	NI ⇌ V	90	5	285.007720	49.503979
August 6th	KOI-3138.01	NI ⇌ R	120	4	292.503780	41.830421
August 7th	KOI-1654.01	NI ⇌ R	180	5	283.796540	49.503990
August 26th	KOI-0882.01	NI ⇌ R	120	5	295.835360	42.943062
August 27th	KOI-0882.01	R ⇌ V	150	5	295.835360	42.943062

Table 1: All observations of KOI's in this study and relevant information is listed here. (NI = near infrared, R = red, V = green, B = blue)

error and flux error disagree significantly). Consequently, standard error was used to calculate the statistical significance of transits (necessary because of low S/N), as opposed to implementing a weighted error (using the flux errors from AIJ).

Although it is common practice to use models for exoplanet LC fitting, this technique was not used. Instead, change-point analysis (CPA) was implemented to identify locations where changes occurred. This allowed LCs to be segmented into three sections: out-of-transit (OOT), transit, and inner-transit (used to calculate transit depth). These sections allowed for the parameterization of LCs (see section 4.2). This method is at a disadvantage to modeling since parameters such as ingress, egress, and transit depth are hard-coded into the model itself. With CPA, we must approximate these values using only the LC data.

4.1 Change-Point Analysis

CPA is a powerful tool for overcoming noisy data to detect even the most subtle changes often missed by other methods. Cumulative sum (CUSUM) charts are at the heart of CPA. The procedure is simple: construct a CUSUM chart of the target and then determine the confidence level of any changes by bootstrapping with more CUSUM charts. First, calculate the mean, $\overline{X}$. Second, the CUSUM is given by:

$$S_i = S_{i-1} + (X_i - \overline{X}) \tag{1}$$

CUSUM charts will always begin and end at zero since the sum of all deviations from the mean is always zero. For this study, ingress and egress times were approximated by using the S_{max} and S_{min} values, respectively (Time of S_{max} = ingress, and time of S_{min} = egress).

This method can be robust with highly scattered LCs, even to the point where previously unseen changes become apparent (see Figure 2). Although S_{max} and S_{min} are typically well defined within a CUSUM chart, there were cases where the rapid drop-off of the S value was not immediately preceded by S_{max} (or succeeded by S_{min}, alternatively). In such scenarios, a second-order CUSUM (CUSUM of change interval only; depicted by the red vertical lines) can be executed to better select the transit period (depicted by the orange vertical lines; see Figure 3).

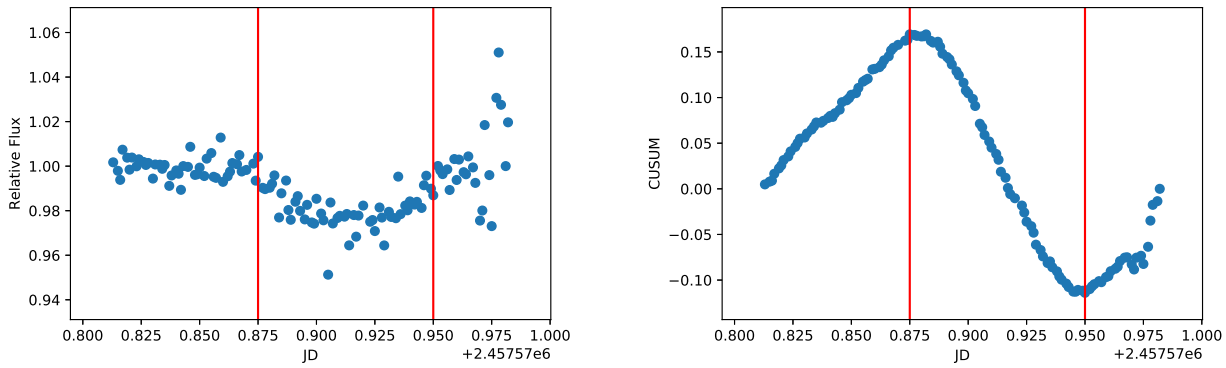

Figure 1: A normalized LC of KOI-1326.01 (left; taken in the red filter) and its corresponding CUSUM chart (right) is shown to demonstrate the clear relation of the CUSUM S_{max} to the ingress (first red line), and the CUSUM S_{min} to the egress (second red line). Outliers in the relative flux plot are not excluded to show how outliers effect the CUSUM plot.

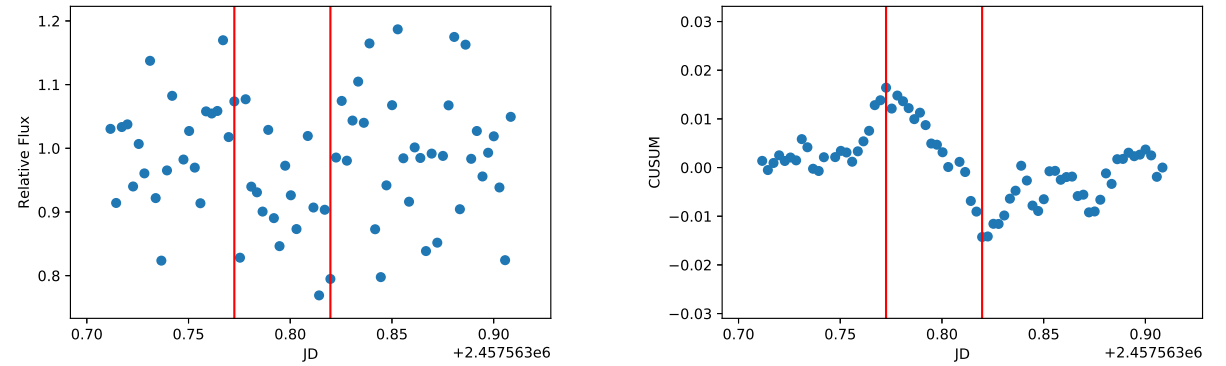

Figure 2: A normalized LC of the first observation of KOI-1654.01(left; taken in the blue filter) and its corresponding CUSUM chart (right) shows just how sensitive CPA is to changes in flux.

4.1.1 Bootstrapping

Bootstrapping allows us to place a level of confidence on any change-interval (change-interval being defined as any duration where a change was occurring, such as a transit). This confidence level will later be used to determine what can or cannot be asserted based off of the data. Random reordering of relative flux plots allowed for additional CUSUM plots to be produced, which we call bootstraps. These bootstraps are then compared to the original data to calculate a confidence level. Since any trends in the original LC are lost because of the reordering, bootstrapped CUSUM plots will tend to remain closer to zero (see Figure 4). The value of interest when bootstrapping is the S_d associated with each CUSUM plot. S_d is simply the largest value minus the lowest value in a given CUSUM plot (refer back to Figure 1). This can be expressed as:

$$S_d = S_{max} - S_{min}, \tag{2}$$

with S_d being for the original LC, and S_d^i $(i = 0, 1, 2, 3, ...N)$ for the bootstraps. For each original LC, one thousand bootstraps were generated using a random sampling function in the Lib/random.py module of

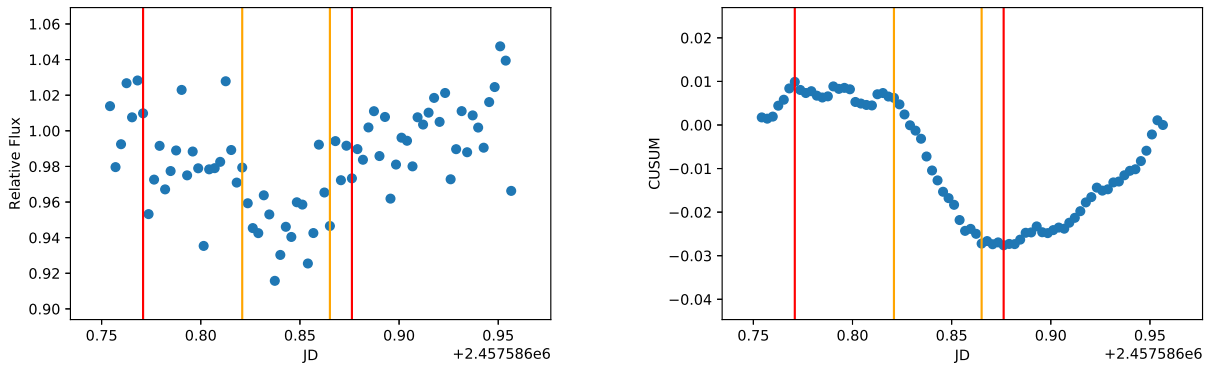

Figure 3: A normalized LC of the second observation of KOI-1654.01 (left; take in the green filter) and its corresponding CUSUM plot (right) is shown to demonstrate how a second-order CUSUM is sometimes required to better select the transit period.

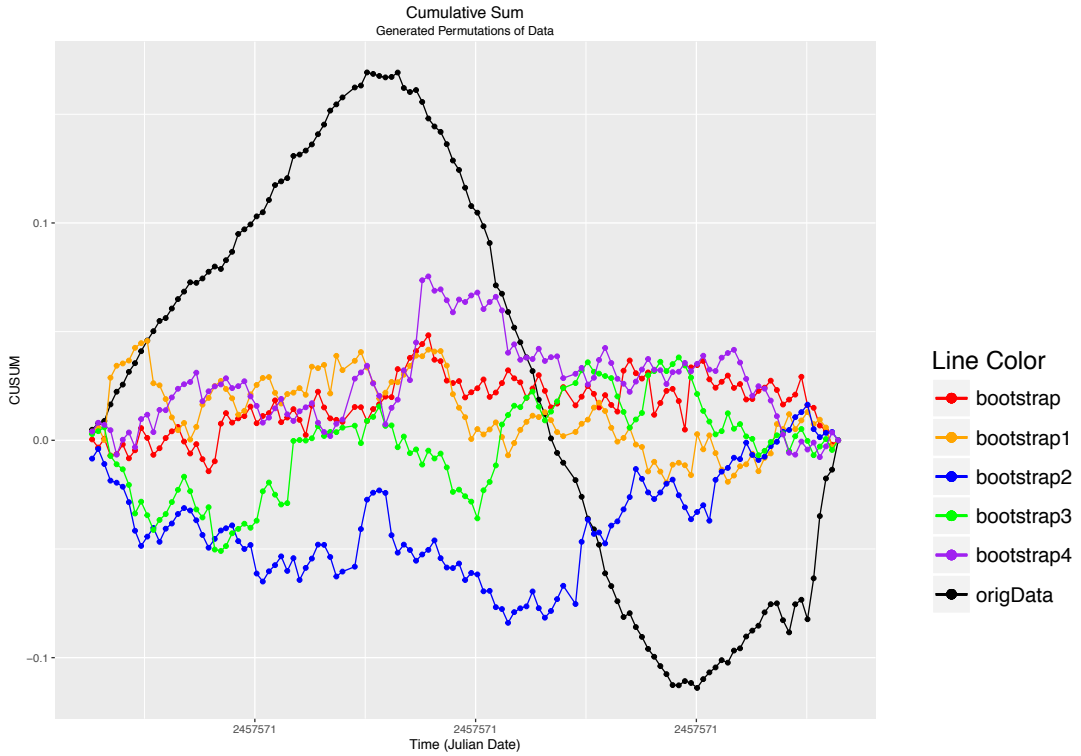

Figure 4: In black, a CUSUM plot of a KOI-1326.01 observation is shown. Five example bootstraps are shown for comparison. Note that one thousand bootstraps were used to calculate the confidence level.

Python. The confidence level (CL) is given by:

$$100\frac{Y}{N}\%. \tag{3}$$

Let Y be the number of bootstraps for which $S_d^i < S_d$, and N be the total number of bootstraps generated. Simply put, S_d is the magnitude of the change, and to get a high CL, we expect nearly all of our bootstraps to have a smaller magnitude of change than our original data. While bootstrapping could be used as an alternative to standard error, bootstrapping was not used to calculate the CL of transit measurements. This study reports bootstrapping (which is typically used with CPA) as a possible alternative for calculating the CL that is worth comparing to standard error.

4.2 Light Curve Segmentation and Parameterization

Figure 5 shows how LCs were segmented. The OOT region was defined as the region outside of the ingress and egress (red vertical lines), and the inner transit was defined as the region inside the orange vertical lines in Figure 5. The inner transit is found by taking the CUSUM of the transit period, and finding the S_{max} and S_{min}. In principle, this should select the region of an LC where values are mostly around the minimum (where it has flattened out, basically). This procedure is necessary since including transition points (due to limb darkening of the star) would reduce transit depth estimates.

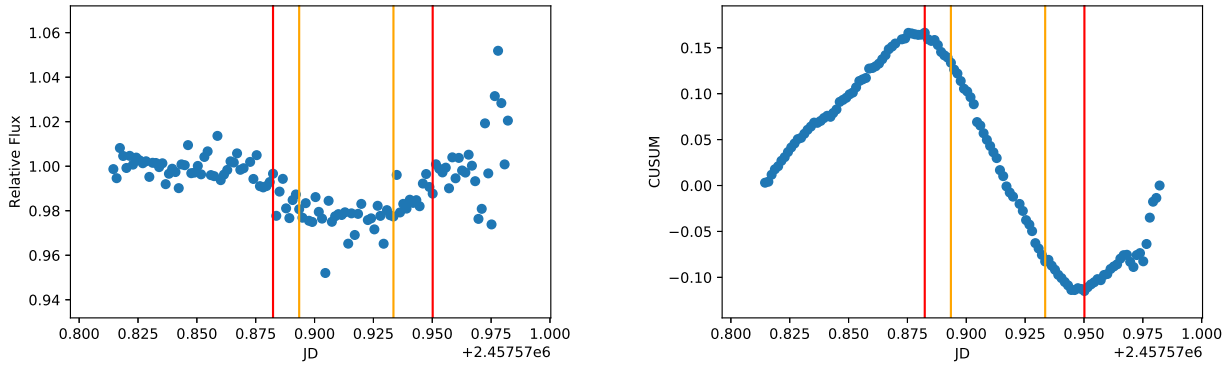

Figure 5: A normalized LC of KOI-1326.01 (left; taken in the red filter) and its corresponding CUSUM chart (right) is shown. The orange lines (S_{max} and S_{min} of second-order CUSUM) enclose the inner transit region used to calculate the transit depth. Not shown is the second-order CUSUM plot.

Transit depth, p (characterized by the planet-star ratio), is calculated with the mean OOT flux, $\overline{X}_{oot}$, and the mean inner transit flux, $\overline{X}_{in}$. Simply:

$$p = 100\frac{\overline{X}_{oot} - \overline{X}_{in}}{\overline{X}_{oot}}\%. \tag{4}$$

An error in p is found with the quadrature sum of the standard error, σ, in both the OOT flux and inner transit flux. Standard error is defined as the standard deviation, s, over the square root of the sample size, n.

$$\sigma_{oot} = \frac{s_{oot}}{\sqrt{n_{oot}}}, \quad \sigma_{in} = \frac{s_{in}}{\sqrt{n_{in}}} \tag{5}$$

And finally,

$$\sigma_p = \frac{\sqrt{\sigma_{oot}^2 + \sigma_{in}^2}}{\overline{X}_{oot}}\%, \tag{6}$$

gives us an error on the transit depth as a percent. The confidence interval (CI) is given by the ratio between the transit depth and its associated error, σ_p. CI was important to calculate since many LCs had very low transit S/N.

5 Results

Relevant measurements for all observations are listed in Tables 2 - 8. Uncertainties for t_o are not given since p and Δp are the values of interest for this study. Confidence intervals for the difference in transit depth ($CI_{\Delta p}$) between filters fail to exceed a 3σ threshold across all observations for all *Kepler* candidates studied. Consequently, assertions about the likelihood of a false positive scenario for these candidates lack statistical weight.

The August 6th observation of KOI-3138 saw no appreciable transit event in the near infrared or red. In the June 21st observation of KOI-3749, the 90 second exposure time was insufficient in the blue filter, and a LC could not be created.

Table 2: KOI-1654.01

Observation	Bandpass	p (%)	CI_p	t_o (HJD)	Δp (%)	$CI_{\Delta p}$
1 (June 23)	R	4.176 ± 0.323	12.9σ	2457563.800	5.850 ± 2.754	2.1σ
	B	10.026 ± 2.735	3.6σ	2457563.796		
2 (July 16)	R	4.413 ± 0.399	11.0σ	2457586.850	0.044 ± 0.858	$< 0.1\sigma$
	V	4.369 ± 0.760	5.7σ	2457586.843		
3 (Aug 7)	R	4.092 ± 0.527	7.7σ	2457608.802	0.655 ± 0.860	$< 0.1\sigma$
	NI	3.438 ± 0.680	5.1σ	2457608.802		

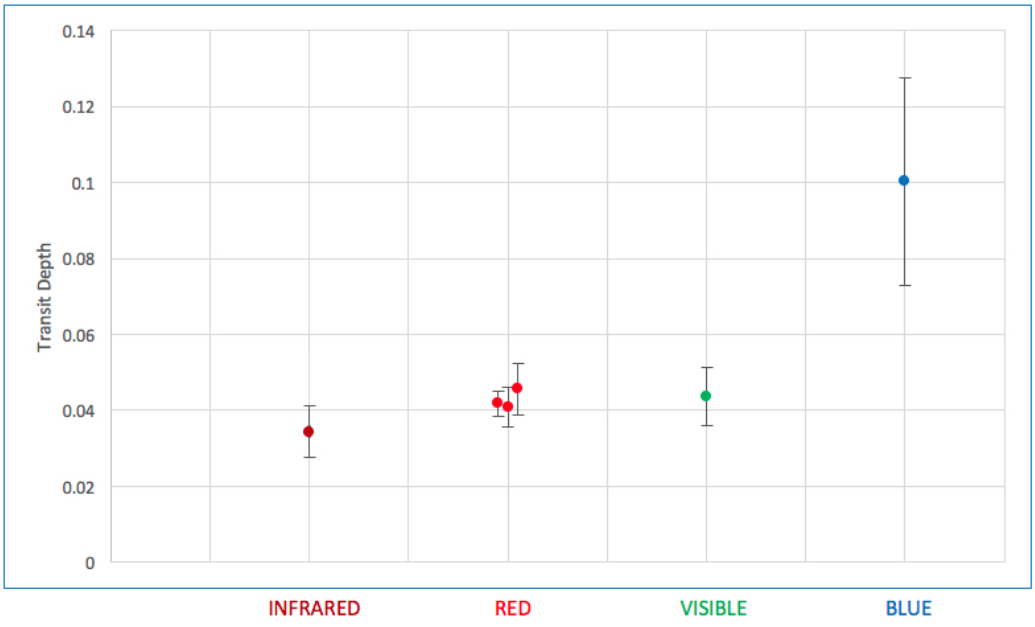

Figure 6: p values from all three observations of KOI-1654.01 show a possible color dependence.

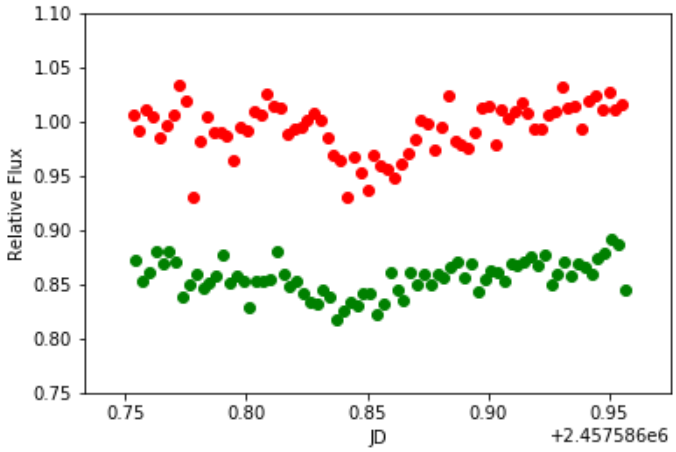

Figure 7: July 16th observation of KOI-1654.01 with red (top) and visible (bottom) filters. LCs are normalized with respect to the red LC OOT mean flux. The visible LC was raised by a constant 0.3 for y-axis scaling purposes.

Table 3: KOI-0882.01

Observation	Bandpass	p (%)	CI_p	t_o (HJD)	Δp (%)	$\text{CI}_{\Delta p}$
1 (Aug 26)	R	3.191 ± 0.442	7.2σ	2457627.771	0.110 ± 0.881	$< 0.1\sigma$
	NI	3.081 ± 0.763	3.7σ	2457627.761		
2 (Aug 28)	R	6.102 ± 1.926	3.2σ	2457629.735	3.671 ± 2.406	1.5σ
	V	2.431 ± 1.442	1.7σ	2457629.756		

Table 4: KOI-3138.01

Observation	Bandpass	p (%)	CI_p	t_o (HJD)	Δp (%)	$\text{CI}_{\Delta p}$
1 (Aug 6)	R	1.878 ± 2.025	0.9σ	2457607.759	x	x
	NI	x	x	x		

Table 5: KOI-3749.01

Observation	Bandpass	p (%)	CI_p	t_o (HJD)	Δp (%)	$\text{CI}_{\Delta p}$
1 (June 21)	R	9.099 ± 1.435	6.3σ	2457561.903	x	x
	B	x	x	x		
2 (Aug 3)	NI	5.400 ± 0.761	7.1σ	2457604.809	0.265 ± 2.128	$< 0.1\sigma$
	V	5.665 ± 1.987	2.9σ	2457604.808		

6 Discussion

Follow-up observations of all seven *Kepler* Objects of Interest in this study fail to demonstrate any statistically significant ($> 3\sigma$) color dependence in transits. Of these seven *Kepler* objects, only KOI-3119.01 and

Table 6: KOI-1326.01

Observation	Bandpass	p (%)	CI_p	t_o (HJD)	Δp (%)	$CI_{\Delta p}$
1 (June 30)	R	2.044 ± 0.136	15.1σ	2457570.913	0.576 ± 0.400	1.4σ
	B	2.620 ± 0.376	7.0σ	2457570.913		

Table 7: KOI-0883.01

Observation	Bandpass	p (%)	CI_p	t_o (HJD)	Δp (%)	$CI_{\Delta p}$
1 (June 22)	R	4.335 ± 0.610	4.3σ	2457562.938	0.202 ± 1.771	$< 0.1\sigma$
	B	4.536 ± 1.662	2.7σ	2457562.926		

Table 8: KOI-3119.01

Observation	Bandpass	p (%)	CI_p	t_o (HJD)	Δp (%)	$CI_{\Delta p}$
1 (July 29)	V	0.336 ± 0.159	2.1σ	2457598.922	0.202 ± 0.282	0.2σ
	NI	0.385 ± 0.233	1.6σ	2457598.942		

KOI-0883.01 have remained as candidates since this study performed observations of them in 2016 (found from the NASA Exoplanet Archive KOI database). For example, KOI-1654.01 was listed as a false positive in March 2017 because of the discovery of a secondary transit event, implying that KOI-1654 is an eclipsing binary. This finding is consistent with the possible color dependence (but does not exceed the 3σ threshold) of the transit depth found in this study (see Figure 6).

The lack of photometric precision required to effectively carry out this study was a result of the low magnitude of KOIs (between V$\sim$15 and V$\sim$18) and small aperture of the SSO telescope (0.61 meters). While this can always be compensated for by increasing the duration of exposures, doing so in excess would create an insufficient time resolution for capturing transit events which may last less than 60 minutes. Additionally, parameters such as the ingress and egress have larger uncertainties with longer exposures. In reflection of the results of this study, multi-color photometry as a way to vet KOIs is not recommended for telescopes with similar specifications to SSOT. Although, this method is likely much more viable for brighter targets, as is common for ground-based exoplanet surveys such as WASP, which analyze stars between V$\sim$9 and V$\sim$13.

The use of change-point analysis in this study to parameterize light curves is an alternative to the conventional modeling technique used by most astronomers. This study does not present CPA as the superior method, but rather an interesting second option that doesn't require any assumptions about the astrophysical (orbital) parameters of a target system. Modeling has constraints based upon the orbital parameters you feed it. These constraints have mostly positive consequences since it guarantees that models will be representative of a real astrophysical scenario. CPA, however, has no such constraints. Parameterization of LCs with CPA is based purely on the information held within those LCs, without invoking the astrophysics of a hypothetical system. To further investigate the efficacy of CPA in LC analysis, a direct comparison must be made to modeling in a future study.

7 Acknowledgments

North Carolina Space Grant for funding this project. NASA Kepler scientist Dr. Steve Howell for providing input on the methodology. Data Science professor Dr. Kevin Sanft for advising the use of change-point analysis. Colleagues Nathan Breedlove, Eliot Dixon, and Matt Lineback for their contribution in Python and R coding. Sierra Stars Observatory Network for access to the Sierra Stars Observatory. Astronomy

professor Jason Kendall of William Paterson University for his guidance and suggestions, as well as putting me in contact with SSON.

References

[1] B. Tingley. Using color photometry to separate transiting exoplanets from false positives. *Astronomy & Astrophysics*, 425(3):1125-1131, 2004.

[2] Colón, Knicole D., and Eric B. Ford. Vetting Kepler Planet Candidates with Multicolor Photometry from the GTC: Identification of an Eclipsing Binary Star Near KOI 565. *Publications of the Astronomical Society of the Pacific*, 123(910):1391-1397, 2011.

[3] Colòn, Knicole D., and Eric B. Ford. Benefits of ground-based photometric follow-up observations for transiting extrasolar planets discovered with Kepler and CoRoT. *The Astrophysical Journal*, 703(1), 2009.

[4] Colòn, Knicole D., et al. Characterizing transiting extrasolar planets with narrow-band photometry and GTC/OSIRIS. *Monthly Notices of the Royal Astronomical Society*, 408(3):1494-1501, 2010.

[5] Timothy D. Morton, et al. False positive probabilities for all Kepler Objects of Interest: 1284 newly validated planets and 428 likely false positives. *The Astrophysical Journal*, 822(2), 2016.